

# Focused Ultrasound Enhances Brain Delivery of Sorafenib Nanoparticles

Daniel Dahis, Dana Meron Azagury, Fadi Obeid, Michelle Z. Dion, Alexander M. Cryer, Mariana Alonso Riquelme, Pere Dosta, Ariel William Abraham, Moshe Gavish, Natalie Artzi,\* Yosi Shamay,\* and Haim Azhari\*

Glioblastoma (GBM) is a universally lethal form of brain cancer. The success of novel treatments is hindered by the blood–brain barrier (BBB), which prevents most drugs from penetrating GBM tumors. Sorafenib (SFB), a proapoptotic multikinase inhibitor, has been investigated for the treatment of GBM; however, survival benefit among patients has not improved. Recently, an indocyanine-stabilized nanoparticulate form of SFB (SFB NPs) with improved tumor accumulation was developed in comparison to SFB alone. Herein, the benefit of SFB NPs and focused ultrasound (FUS)-mediated BBB disruption is assessed to enable noninvasive, safe, and reversible BBB permeation for enhanced SFB NPs brain accumulation. Treatment of SFB NPs and FUS yields lower IC<sub>50</sub> values (2.7 and 29 μm in 2D and 3D U87 cell models vs 7.5 and 37.1 μm for SFB NPs alone). SFB NPs and FUS with microbubbles improve SFB NPs uptake by U87 cells compared to SFB NPs alone (46% increase;  $p = 0.0123$ ). In vivo, FUS enhances SFB NPs brain accumulation by 2.5-fold compared to the contralateral hemisphere, and 3.6-fold compared to unsonicated brains. In conclusion, SFB NPs are a promising agent for GBM treatment and its therapeutic capacity can be potentially enhanced when combined with FUS-mediated BBB disruption.

## 1. Introduction


Glioblastoma (GBM) is the most common form of primary malignant brain cancers in adults, accounting for over 50% of gliomas in the United States.<sup>[1,2]</sup> GBM is particularly aggressive and frontline treatment consists of surgical resection followed by concurrent temozolomide chemotherapy (TMZ), radiation therapy (RT), and corticosteroids.<sup>[3]</sup> Yet, the median survival of GBM patients remains less than 20 months, a statistic that has not changed substantially in the last 20 years.<sup>[4–6]</sup>

A major challenge in GBM treatment is to effectively deliver drugs to the tumor site across the highly selective blood–brain barrier (BBB). In an orchestrated operation, the BBB prevents the penetration of most water-soluble drugs with molecular size greater than 400 Da (>2 nm) into the brain parenchyma.<sup>[7]</sup> Consequently, it is estimated that 98% of small molecule

drugs and all large molecule drugs do not have access to the central nervous system (CNS).<sup>[8]</sup> Yet, the BBB can be compromised by GBM tumors, leading to regions with increased leakiness.<sup>[9]</sup>

D. Dahis, D. M. Azagury, Y. Shamay, H. Azhari  
Department of Biomedical Engineering  
Technion Institute of Technology  
Haifa 3200003, Israel  
E-mail: yshamay@bm.technion.ac.il; haim@bm.technion.ac.il

D. Dahis, M. Z. Dion, A. M. Cryer, M. A. Riquelme, P. Dosta,  
A. W. Abraham, N. Artzi  
Department of Medicine  
Engineering of Medicine Division  
Brigham and Women's Hospital  
Harvard Medical School  
Cambridge 02115, MA, USA  
E-mail: nartzi@mit.edu

 The ORCID identification number(s) for the author(s) of this article can be found under <https://doi.org/10.1002/anbr.202200142>.

© 2022 The Authors. Advanced NanoBiomed Research published by Wiley-VCH GmbH. This is an open access article under the terms of the Creative Commons Attribution License, which permits use, distribution and reproduction in any medium, provided the original work is properly cited.

DOI: 10.1002/anbr.202200142

D. Dahis, M. Z. Dion, A. M. Cryer, P. Dosta, N. Artzi  
Wyss Institute for Biologically Inspired Engineering  
Harvard University  
Boston, MA 02115, USA

F. Obeid, M. Gavish  
The Ruth and Bruce Rappaport Faculty of Medicine  
Technion Institute of Technology  
Haifa 31096, Israel

M. Z. Dion, A. M. Cryer, P. Dosta  
Institute for Medical Engineering & Science  
MIT  
Cambridge 02139, MA, USA

N. Artzi  
Broad Institute of Harvard and MIT  
Cambridge, MA, USA

This phenomenon permits penetration of certain drugs, particularly at the nanosize scale.<sup>[7,8]</sup>

A promising class of antitumor drugs are kinase inhibitors<sup>[10,11]</sup> such as sorafenib (SFB).<sup>[12,13]</sup> SFB is currently approved by the Food and Drug Administration (FDA) for the treatment of patients diagnosed with hepatocellular carcinoma (HCC) and renal cell carcinoma (RCC) and is currently being investigated in clinical trials for the treatment of GBM due to its antitumor capabilities that include blocking tumor proliferation, angiogenesis, and tumor cell apoptosis. Specifically, SFB works by inhibiting multiple kinases such as platelet-derived growth factor receptor  $\beta$  (PDGFR $\beta$ ), vascular endothelial growth factor 2 and 3 (VEGF), FMS-like tyrosine kinase 3 (FLT3), and the receptor tyrosine kinase c-KIT.<sup>[14,15]</sup> Shamay et al. recently developed a dye-stabilized nanoparticle (NP) platform, based on nanoprecipitation of hydrophobic drugs coassembled with fluorescent, sulfated, indocyanine dyes. In this platform, the self-assembly process relies on both hydrophobic and pi-pi interactions between the indole groups of IR783 and the aromatic groups of the hydrophobic drugs. In addition, it was shown that the drugs having high number of intrinsic state subgroups such as double bonded oxygen and fluorine atoms further stabilize the NP. When combined with the indocyanine IR783 dye, these hydrophobic drugs increased solubility about 2000-fold, resulting in a complete suspension of sub-100 nm drug-dye nanoparticles (SFB NPs).<sup>[13]</sup> SFB NPs depicted high drug loading efficiency (>85%), sustained SFB release for over 48 h, high serum stability, and improved pharmacokinetics when compared to SFB in its free form. When employed for the treatment of a murine HCC model, SFB NPs successfully induced tumor eradication and substantially prolonged survival.<sup>[13]</sup>

Notably, GBM tumors express high levels of VEGF and VEGF receptors, mitogen-activated protein kinase (MAPK), and PDGFR activation; about 30% of patients carry an amplicon on chromosome 4q12 comprising VEGFR2, PDGFR- $\alpha$ , and KIT genes.<sup>[16]</sup> Thus, multikinase inhibition is promising for GBM treatment, as demonstrated in a preclinical setting.<sup>[17]</sup> However, so far, when administered in its free form, survival benefit among GBM patients has not significantly improved,<sup>[18–20]</sup> in part due to the low levels of SFB crossing the BBB and reaching the tumor.<sup>[21,22]</sup> Nanoparticulated drugs such as SFB NPs, in turn, may address this issue, by improving selectivity, accumulation, and persistence of the drug in the tumor microenvironment (TME).<sup>[23]</sup> Importantly, SFB NPs components, SFB and IR783, are FDA-approved (in the case of SFB) and indocyanine dyes have been extensively studied and are currently in clinical trials in human patients.<sup>[24–26]</sup> However, mechanisms of drug expulsion from the BBB such as the active efflux of penetrating molecules<sup>[7]</sup> remain intact, thereby highlighting the need of additional modalities able to permeate the BBB.

In this sense, multiple investigations of novel methods for crossing or bypassing the BBB have been suggested. These include the local administration of drugs into the brain,<sup>[27,28]</sup> leveraging receptor-mediated transcytosis of drugs through the BBB using targeted nanomedicines,<sup>[29,30]</sup> the use of hyperosmotic solutions,<sup>[31,32]</sup> and intranasal and intratympanic delivery of drugs,<sup>[33,34]</sup> among others.<sup>[8,35]</sup> Although these strategies represent advances in drug delivery to the CNS, they are often

nonselective, invasive, and may be followed by undesired side effects.<sup>[36]</sup>

Acoustic treatments employing focused ultrasound (FUS) have been shown to be selective and able to safely and noninvasively improve the penetration of drugs into tumors.<sup>[37–39]</sup> The seminal work by Hynynen et al. demonstrated the benefits of including ultrasound contrast agents (i.e., microbubbles [MBs] 1–10  $\mu\text{m}$  in diameter) in transcranial FUS protocols,<sup>[40]</sup> which allowed for the selective disruption of the BBB with relatively low acoustic powers. This approach was proven to be safe and reproducible, even after multiple treatment sessions, with demonstrated improved brain delivery of nanomedicines with molecular size of up to 200 nm.<sup>[38,41–45]</sup>

Hence, this study investigated the therapeutic potential of SFB NPs in the context of GBM treatment (U87-luc) and assessed its uptake *in vitro* and accumulation in the brain when combined with FUS-mediated BBB disruption *in vivo*. Our results demonstrate that SFB NPs are potent in reducing cell viability of 2D and 3D human GBM cell cultures. The combination of SFB NPs with FUS sonication enhanced NPs uptake by GBM cells. *In vivo*, the brain accumulation of SFB NPs was significantly higher when combined with FUS. Our results depict, for the first time, the therapeutic potential of SFB NPs and its combination with FUS-mediated BBB disruption as a viable treatment strategy for brain tumors.

## 2. Results

### 2.1. Particle Characterization

Size and charge measurements of SFB NPs were obtained. On average, NPs measured  $88.37 \pm 0.49$  nm (PDI = 0.012) in size and a zeta potential of  $-29.1 \pm 2.4$  mV. Drug loading and encapsulation efficiency were, respectively, 82% and 88% as measured via high-performance liquid chromatography (HPLC) (Figure 1a, b). As previously demonstrated (Shamai et al.), SFB was released from SFB NPs following 48 h in PBS incubation.<sup>[13]</sup> The NPs were stable for 7 days in room temperature, at  $2 \text{ mg mL}^{-1}$  concentration (Figure 1c; Figure S1, Supporting Information). Cryo-transmission electron microscopy (TEM) confirmed their morphology (Figure 1d). The measured critical micelle concentration (CMC) for the NPs was of  $5\text{--}10 \mu\text{g mL}^{-1}$  and long-term storage was achieved with freeze-drying in the presence of 5% sucrose as cryoprotectant. In this form, the particles were stable for more than 12 months (Figure S2, Supporting Information). U87 cells coincubated with increasing concentrations of SFB NPs effectively internalized the particles as observed via flow cytometric analysis (Figure 1e–f), depicting 1.9- and 4.5-fold increase in APC-Cy5 expression (SFB NPs) by cells treated with 2 and  $10 \mu\text{g mL}^{-1}$ , respectively, when compared to untreated U87 cells.

### 2.2. Cell Viability in a 2D and Spheroidal GBM Models Following SFB NPs or SFB Treatment

The anticancer efficacy of SFB NPs was evaluated by assessing the viability of U87 cells *in vitro* following drug exposure. U87 cells were exposed to multiple concentrations of SFB NPs or free

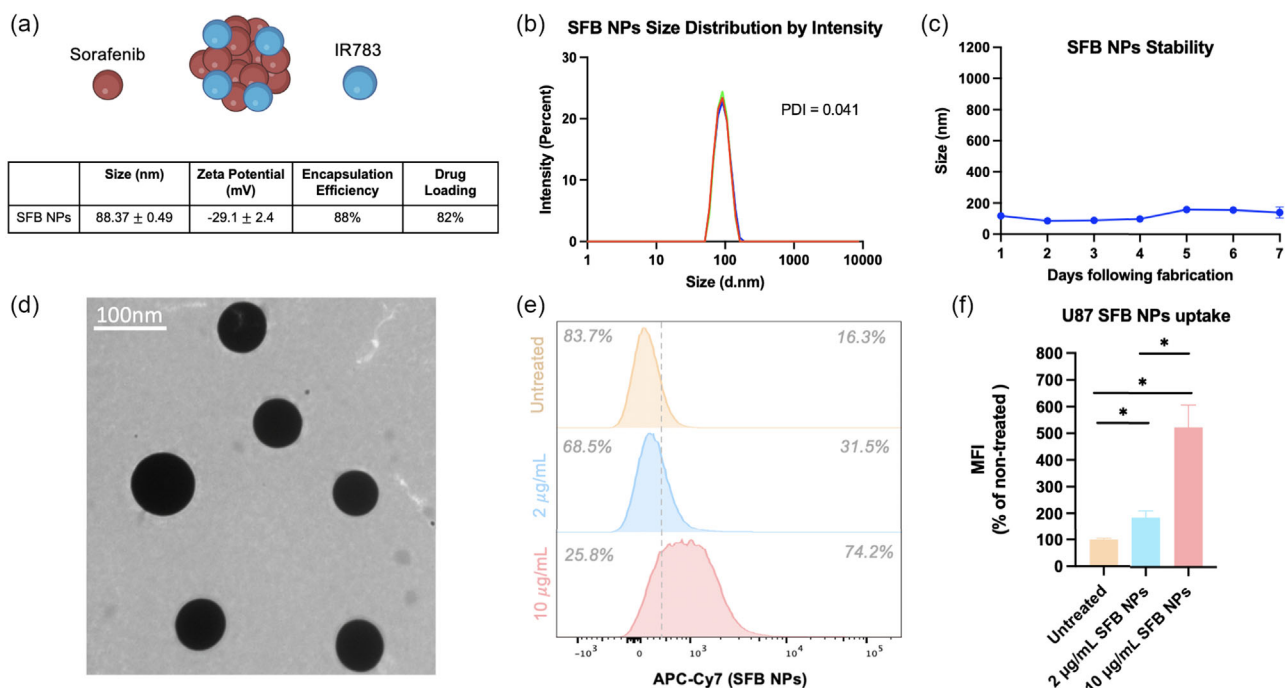


**Figure 1.** a) SFB NPs characterization. b) DLS measurement of size distribution by intensity. c) Stability of SFB NPs. d) TEM images of the NPs. e) Normalized histograms of U87 cells treated with increasing concentrations of SFB NPs (0, 2, or 10  $\mu\text{g mL}^{-1}$ ). Percentages represent the average values for negative (left) and positive (right) colocalization of SFB NPs and U87 cells. f) SFB NPs uptake quantification. Data are expressed as mean  $\pm$  SEM,  $n = 3$ ,  $*p < 0.05$ .

SFB ranging from 28 nm to 185.3  $\mu\text{M}$  (Figure 2). The obtained half-maximal inhibitory concentration ( $\text{IC}_{50}$ ) for SFB NPs and free SFB in 2D cultures was of 7.5 and 2.3  $\mu\text{M}$ , respectively (Figure 2a). Treatment of dye alone was not cytotoxic at these molarities ( $\text{IC}_{50\text{dye}} = 74.4 \mu\text{M}$ ), suggesting that the cytotoxic effect is primarily driven by SFB (Figure S3, Supporting Information). SFB NPs and SFB treatment effectively induced higher apoptotic levels of U87 cells as observed via flow cytometric and microscopy analysis (Figure S4, Supporting Information).

Next, we determined the cytotoxicity of SFB NPs using U87-derived spheroids (Figure 2b). The obtained  $\text{IC}_{50}$  values for SFB NPs and free SFB in this case were of 37.1 and 13.3  $\mu\text{M}$ , respectively (Figure 2c). In both cultured models, automated fluorescence microscopy was used to visually assess cell morphology with and without SFB NPs treatment. The obtained images 72 h postdrug exposure depicted effective cell death for the 2D cultures (Figure 2d) and dissociation of 3D spheroids into single cells (Figure 2e) following treatment.

### 2.3. Assessment of Temporal SFB NPs Transcranial Signal in GBM-Bearing Mice

We have previously investigated important aspects related to SFB NPs therapy, including distribution and pharmacokinetics, depicting no signs of NPs cytotoxicity in vivo.<sup>[13]</sup> Here, we investigated the biodistribution and intracranial accumulation of SFB NPs in orthotopic GBM tumors following systemic administration (IP) in a pilot study (Figure 3, S8, Supporting Information).

Mice were intracranially inoculated with U87 tumors and were divided into two groups: untreated or treated with two intraperitoneal doses of SFB NPs (30  $\text{mg kg}^{-1}$ ) on days 7 and 14 posttumor inoculation. The fluorescence efficiency from the brain cavity was measured across different time-points following the second SFB NPs injection (Figure 3a,b). Preliminary assessment of tumor growth and survival depicted a benefit of SFB NPs in delaying tumor growth and promoting median survival of 44.5 days (Figure S5, Supporting Information). At day 29 postinoculation, approximately 15 days following the second SFB NPs treatment, fluorescence signals from the intracranial cavity were still detectable ( $4.3 \pm 0.9\%$ ; normalized to the fluorescent obtained immediately following the second injection). No changes in behavior or body weight loss were observed in treated animals (Figure 3c).

### 2.4. In Vitro SFB NPs Combination with FUS

The effect in cell uptake of incorporating ultrasound sonication along with SFB NPs or SFB treatment was next assessed. Acoustic treatment of SFB NPs did not alter the NPs properties (Figure 4a). When applied to 2D cell cultures, the combination of FUS + SFB NPs reduced cell viability, yielding an  $\text{IC}_{50}$  value of 2.7  $\mu\text{M}$  compared with 7.5  $\mu\text{M}$  for SFB NPs only. When applied to a spheroidal model, FUS protocol + SFB NPs treatment yielded an  $\text{IC}_{50}$  value of 29  $\mu\text{M}$  compared to 33.8  $\mu\text{M}$  for SFB NPs only (Figure 4b–d). A similar trend was observed for free SFB treatment with FUS, depicting an  $\text{IC}_{50}$  value of 2.05  $\mu\text{M}$  for

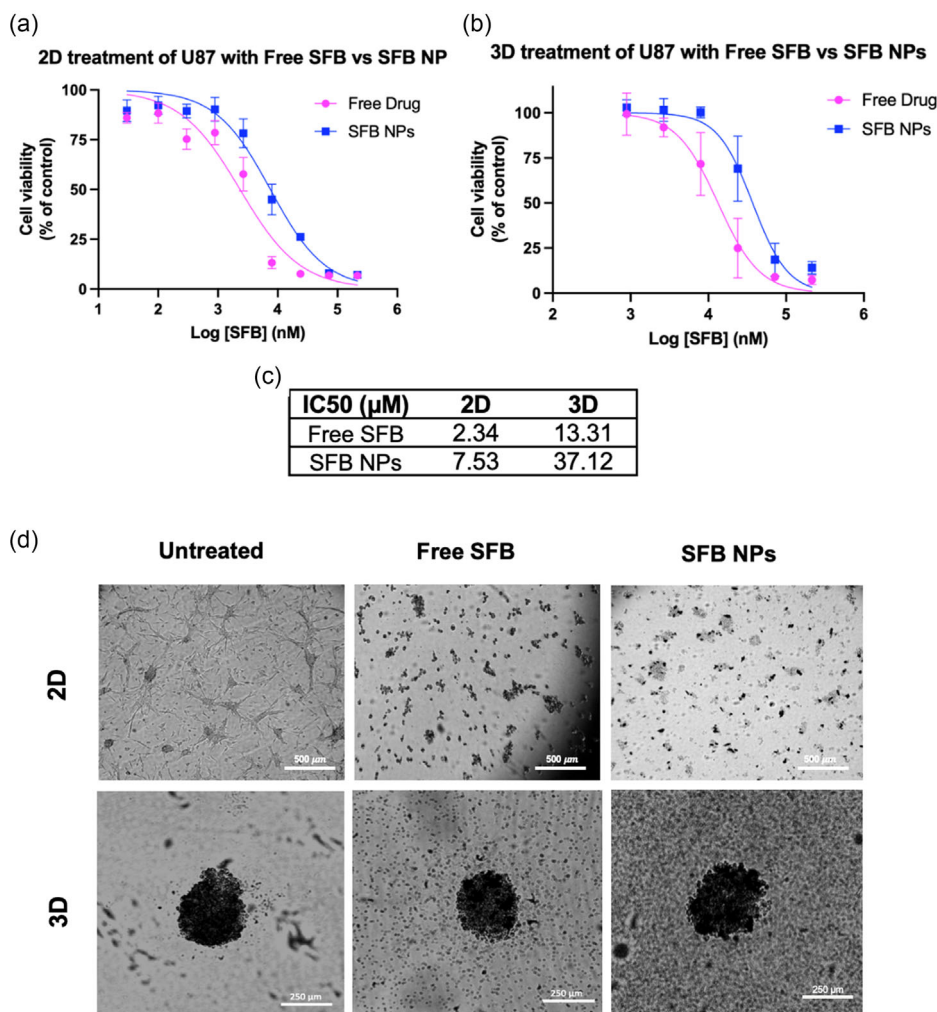


**Figure 2.** U87 Viability upon SFB NPs and free SFB treatment in a) 2D and b) 3D cultures. c) Table summarizing the obtained IC<sub>50</sub> values. Morphological assessment of SFB NPs treatment in d) 2D and 3D cultures. Images displaying cells treated with 0.1 mg mL<sup>-1</sup> SFB or SFB NPs. Data are expressed as mean ± SEM, *n* = 3.

SFB + FUS compared to 2.34 μM for free SFB in the case of 2D cultures, and 10.2 μM compared to 13.3 μM for SFB only treatment in 3D cultures (Figure S6, Supporting Information). Importantly, implementing the FUS protocol alone did not statistically reduce cell viability of 2D and 3D cultures (Figure S7, Supporting Information). These results suggest that FUS application does not impair SFB NPs efficiency and may sensitize U87 cells to SFB NPs therapy.

The effects in NPs uptake of combining FUS sonication with MBs commonly used in FUS-mediated BBB disruption procedures and SFB NPs were next assessed (Figure 4f). Cells receiving FUS + MBs + SFB NPs treatment demonstrated 1.46-fold increase in the percentage of U87-expressing APC Cy7 dye (SFB NPs) in comparison to cells receiving SFB NPs treatment alone. This suggests enhanced NPs internalization following acoustic treatment in comparison to cells receiving NPs treatment alone. Interestingly, we noted that spheroids receiving FUS sonication with MBs (FUS BBBD) and SFB NPs depicted increased dissociation levels in comparison to controls

(Figure 4g), as observed by an increase in spheroidal area (Figure 4h).

Collectively, these results suggest that SFB NPs demonstrate comparable efficacy as SFB alone, and when combined with FUS, FUS sonication with MBs can increase the penetration of SFB NPs into tumor cells and spheroids.

## 2.5. FUS-Mediated BBB Disruption Affect SFB NPs Brain Penetration

To assess the brain penetration of SFB NPs following FUS-mediated BBB disruption treatment, mice underwent FUS-mediated BBB disruption in the left brain hemisphere and SFB NPs intravenous administration while a control group received only SFB NPs (Figure 5a). The enhancement in fluorescence in the left hemisphere was compared with the right hemisphere (nontargeted) of the treated mice, and also compared against the fluorescence detected from hemispheres of

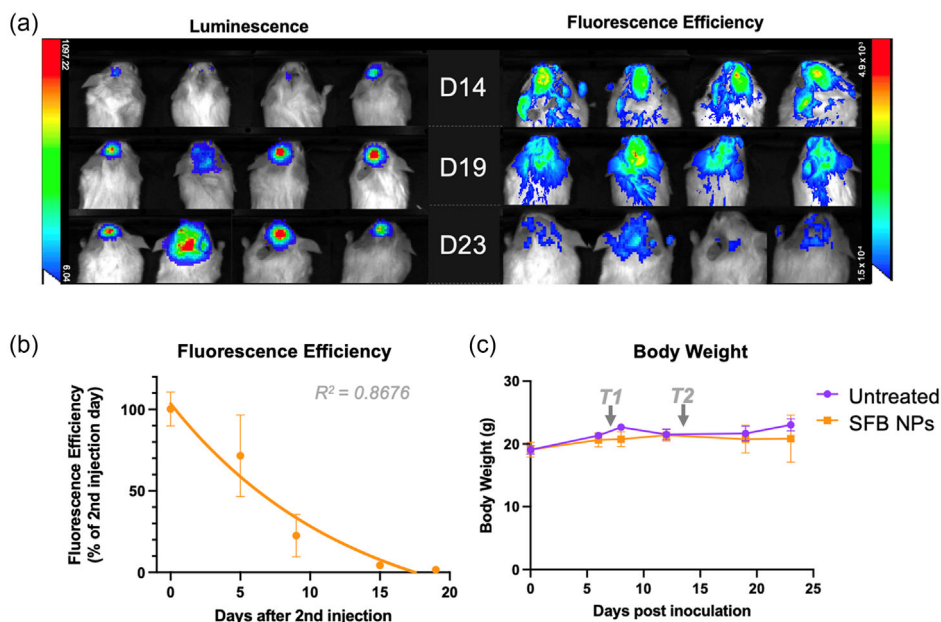


**Figure 3.** Preliminary assessment of SFB NPs treatment in GBM tumors in vivo. a) Bioluminescence (left) indicating tumor location and the corresponding fluorescence indicating the SFB NPs colocalized accumulation (right) subsequent to the second SFB NPs injection. b) The residual measured fluorescence decayed until day 20 post-SFB NPs second injection depicting an exponential decay ( $R^2 = 0.8676$ ) ( $n = 4$  for days 0, 5, 9; and  $n = 3$  for days 15 and 19, postsecond injection). c) Body weight plot of SFB NPs treatment versus control ( $n = 4$  SFB NPs;  $n = 3$  untreated). Datapoints are expressed in mean  $\pm$  SD.

unsonicated mice treated with SFB NPs only. Fluorescence efficiency detected in the targeted hemisphere was 2.47-fold higher than in the untargeted contralateral hemisphere (Figure 5b). When compared to unsonicated brains, the increase in fluorescence was of 3.64-fold, indicating the prominent effect of the FUS sonication and increased SFB NPs brain penetration (Figure 5c). Cross-sectional (Figure 5f) analysis of treated brains revealed an average of  $237.86 \pm 38.31\%$  increase in fluorescence in comparison to the contralateral hemisphere (Figure 5g).

To order to assess the SFB NPs extravasation to the neuroparenchyma following FUS treatment, fluorescent microscopy was used. Brain sections of unsonicated and sonicated mice receiving SFB NPs were scanned. Notably, in contrast to the brain treated with SFB NPs only (Figure 5e) a clear extravasation of SFB NPs from the vasculature was observed in the targeted zone (marked in yellow), when compared to the contralateral, nontargeted hemisphere (Figure 5d). The fate of the administered SFB NPs in combination with the ultrasonic treatment was also assessed by studying the global biodistribution. The detected fluorescence efficiency was variable across different organs (Figure S7, Supporting Information), with preferential accumulation in the lungs, liver, and kidneys.

### 3. Discussion

Cancer treatments have dramatically improved as a result of advances in oncology, personalized medicine, and imaging during the last decades. Yet, the median survival rates for GBM patients have remained at less than 20 months for the last 20 years.<sup>[4–6]</sup> The development of effective GBM treatments faces

multiple challenges. One of these is the presence of the BBB, which protects the tumor against systemically administrated drugs. Hence, overcoming this hurdle is essential for improving therapeutic outcomes. SFB, a multikinase inhibitor used in HCC and RCC, has reached clinical trials for GBM. Nonetheless, so far, the outcomes have been incremental.<sup>[21,46]</sup> Hence, our overarching hypothesis was that a novel nanoparticulated SFB formulation could exert anti-GBM effects, and can obtain increased brain penetration when combined with ultrasound.

We assessed SFB NPs cytotoxicity using a 2D and 3D cell culture models. The obtained  $IC_{50}$  for 2D U87 cultures treated with SFB NPs and SFB was of 7.5 and 2.3  $\mu\text{M}$ , respectively. This range is similar to  $IC_{50}$  measurements observed in other GBM cell lines,<sup>[47]</sup> and comparable to the ones reported before for free SFB in U87 cells.<sup>[17,48]</sup> When applied to a spheroidal U87 model, SFB NPs and SFB only  $IC_{50}$  values were of 33.8 and 13.3  $\mu\text{M}$ , respectively. Expectedly, a difference between the  $IC_{50}$  inhibitory measurements between the 2D and 3D cell models was observed, corroborating previous reports depicting higher  $IC_{50}$  measurements for 3D models in comparison to the 2D ones, in the context of chemotherapy screening.<sup>[49,50]</sup> Also, a difference in the  $IC_{50}$  values for SFB and SFB NPs for both 2D and 3D models was noted. This in vitro difference is characteristic to nanoparticulated drugs and may be related to the mechanism of cell internalization of the drug in its free form (free diffusion) and in a nanoparticulated form (primarily caveolin-mediated endocytosis).<sup>[13,51]</sup> Yet, overall, despite the described difference, SFB stabilization in a nanoparticle form retained similar cytotoxicity than SFB in free form as confirmed by similar apoptotic levels of U87 cells treated

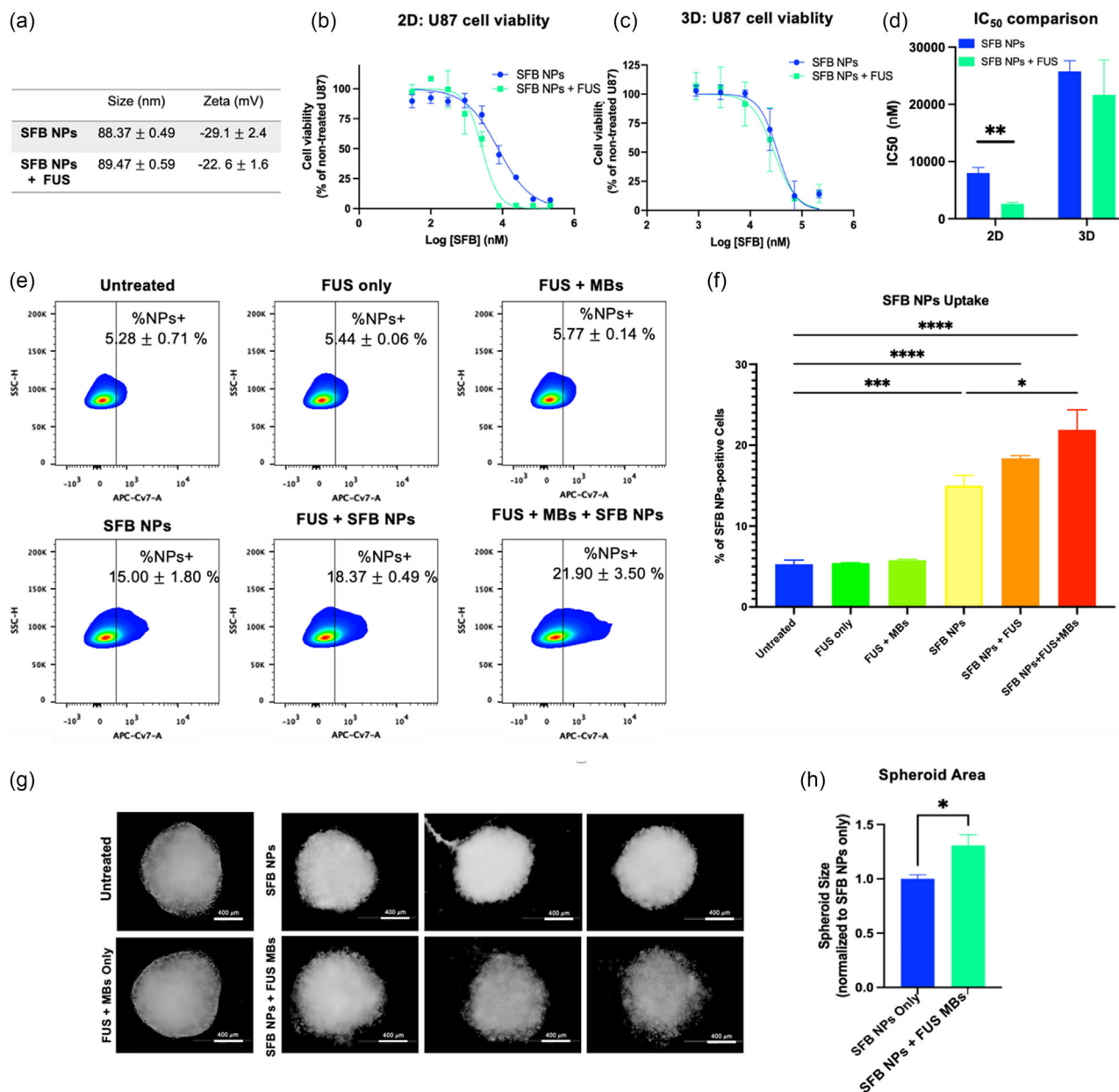


**Figure 4.** In vitro effects of free SFB and SFB NPs combined with FUS. a) Table depicting no significant difference in the NP properties due to FUS sonication. b) 2D cell viability curves for SFB NPs with FUS. c) 3D cell viability curves for SFB NPs with FUS. d) Comparison of IC<sub>50</sub> values for 2D and 3D cultures treated with SFB NPs. e) Flow cytometric scattered plot of cells treated with SFB NPs and FUS. f) Cell NPs uptake quantification between treated groups. SFB NPs were administered at a fixed concentration of 2 μg mL<sup>-1</sup>. g) U87 spheroids 48 h post-SFB NPs (0.1 mg mL<sup>-1</sup>) treatment or SFB NPs + FUS + MBs treatment. h) Spheroidal area quantification 48 h posttreatment. Data are expressed as mean ± SEM, *n* = 3, \**p* < 0.05, \*\**p* < 0.01; \*\*\**p* < 0.001, \*\*\*\**p* < 0.0001.

with SFB NPs and dose-matched SFB, suggesting the preservation of drug potency.

Interestingly, the incorporation of an ultrasonic treatment led to a statistical reduction in the measured IC<sub>50</sub> values for SFB NPs and free SFB in both the 2D- and 3D-U87 culture models. Also, FUS application in combination with MBs statistically increased nanoparticle uptake. These effects could be partially explained by the membrane transient permeabilization capability of ultrasonic

waves which has been described previously,<sup>[52–54]</sup> an effect termed sonoporation. The transient nature of sonoporation provides a window of opportunity for extracellular molecules to penetrate the targeted cells. Following sonication, the membrane integrity of the targeted cells is restored, entrapping drugs intracellularly.<sup>[52]</sup> Also, spheroids treated with SFB NPs and FUS MBs depicted higher dissolution levels (measured via the spheroid area), suggesting that FUS + MBs may have sensitized the

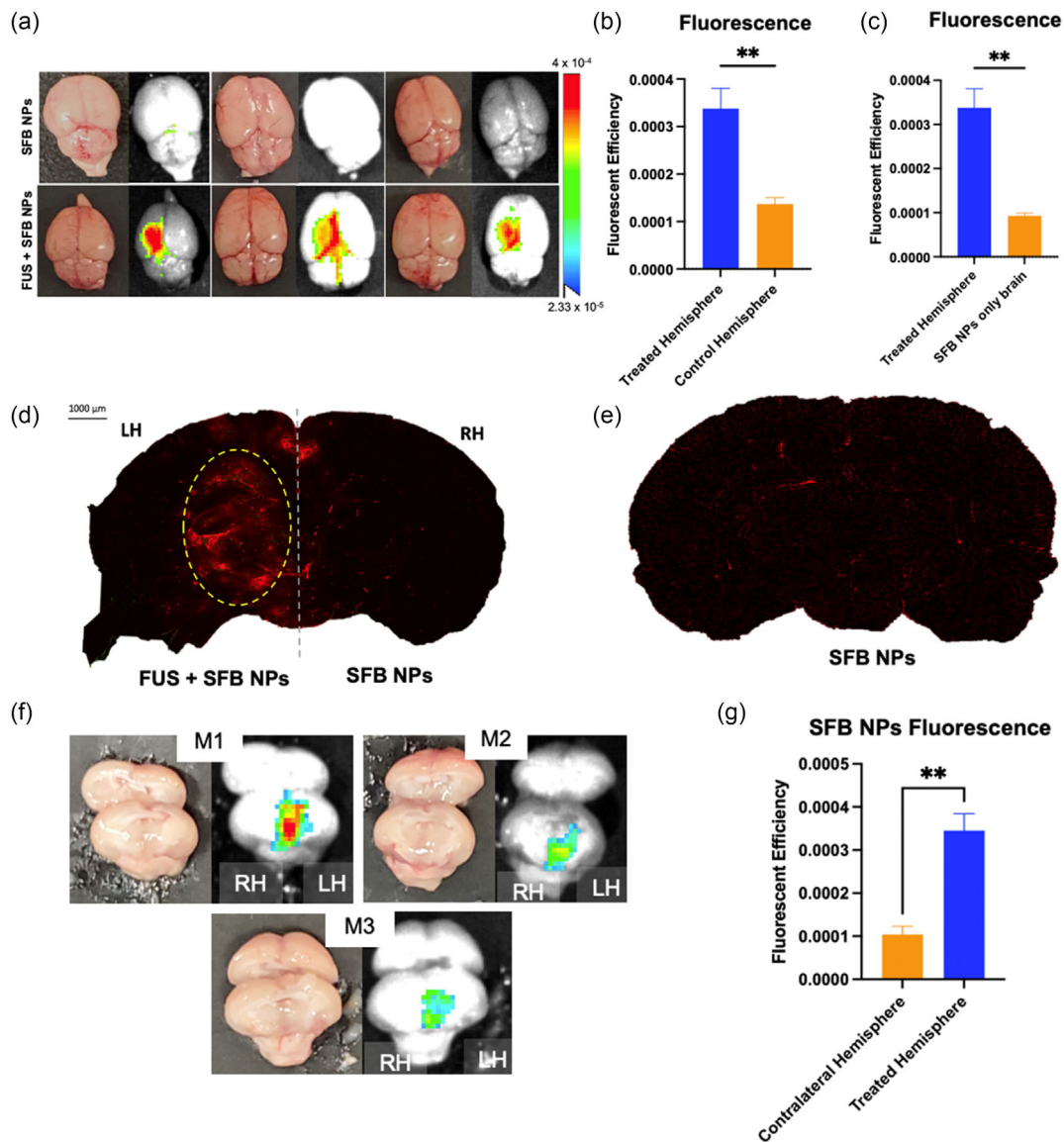


**Figure 5.** FUS-mediated BBB disruption improves SFB NPs penetration into the neuroparenchyma. a) Fluorescence efficiency panel of brains treated with FUS BBB disruption following SFB NPs injection (left) versus brains treated with SFB NPs alone (right). Images taken approximately 1 h posttreatments. Color range is optimized to maximize the contrast between SFB NPs presence in FUS-treated brains. Therefore, the lower presence of SFB NPs in unsonicated brains is not visible in this color scale. b) Quantification of the fluorescence efficiency of the left hemisphere (treated) in comparison to the contralateral hemisphere. c) Quantification of the fluorescence efficiency of the left hemisphere in comparison to the brains treated with SFB NPs alone (control—"CTL"). d) A slide of a mouse treated with FUS BBB disruption and SFB NPs and e) SFB NPs only. f) IVIS images of cross-sectional brain slices of brains treated with FUS and SFB NPs. (f) Treated brain cross sections. g) Quantification of the fluorescence efficiency of the treated cross sections. Data are expressed as mean  $\pm$  SEM,  $n = 3$ ,  $*p < 0.05$ ,  $**p < 0.01$ ;  $***p < 0.001$ .

spheroids to SFB NPs. In vivo, SFB NPs treatment was tolerable, and its fluorescence colocalized with the tumor region. This transcranial signal may be tied to particular features of GBM tumors such as the somewhat permeable BBB, which allows for the accumulation of NPs in the tumor bed via the enhanced permeability and retention effect (EPR).<sup>[55,56]</sup> SFB NPs treatment in vivo promoted delayed tumor growth and improved median overall survival of tumor-bearing animals (44.5 days) after two doses (1 dose week<sup>-1</sup>), a clear improvement compared median

survival of less than 30 days for untreated mice, as previously reported.<sup>[57–59]</sup>

We next studied FUS-mediated BBB disruption and SFB NPs delivery to the brain, assessing the cerebral accumulation of SFB NPs posttreatment. This is particularly relevant in the context of GBM as FUS treatments in BBB disruption mode for improved drug delivery are currently under evaluation in clinical trials for GBM patients (NCT03626896, NCT03551249, NCT04528680). Here, the observed SFB NPs enhancement in the brain

fluorescence signal following FUS-mediated BBB disruption ranged from 2.47-fold when compared with the contralateral, unsonicated hemisphere to 3.67-fold when compared to unsonicated brains. Cross-sectional analysis of treated brains revealed 3.36-fold increase in signal compared to the untreated hemisphere. Apart from the brain, biodistribution analysis revealed no major differences in the distribution profile between animals receiving either SFB NPs or SFB NPs and FUS-mediated BBB disruption, with increased SFB NPs accumulation in the lungs, liver, and kidneys. This observation is in agreement with our previous studies that demonstrated preferential SFB NP accumulation in organs that overexpress caveolin.<sup>[13]</sup> Where organs that overexpress caveolin depict preferential nanoparticle accumulation. Overall, these results highlight SFB NPs potential for future GBM applications in combination with FUS-mediated BBB disruption.

#### 4. Conclusions

This work demonstrates that SFB in its nanoparticulated form can serve as a potent anti-GBM nanomedicine. Overall, SFB NPs preserved the cytotoxicity of SFB, and its combination with FUS and MBs was able to improve uptake by U87 cells. SFB NPs combined with FUS-mediated BBB disruption in vivo were effective in increasing the levels of SFB NPs to the targeted brain. In conclusion, SFB NPs exert potent anti-GBM effects, and its therapeutic accumulation to the brain can be augmented when combined with ultrasound. Overall, these findings may offer a novel strategy for future GBM treatments.

#### 5. Experimental Section

**SFB Nanoparticles Preparation and Characterization:** SFB NPs were synthesized by the following protocol, which is described in detail in Shamay et al.<sup>[13]</sup> Briefly, 200  $\mu\text{L}$  of SFB dissolved in DMSO (10  $\text{mg mL}^{-1}$ ) was added to a 200  $\mu\text{L}$  IR783 aqueous solution (Sigma-Aldrich, 2  $\text{mg mL}^{-1}$ ) and 500  $\mu\text{L}$  0.1 M sodium bicarbonate or deionized water. The additions were performed under slight vortexing. The resulting solution was centrifuged (30 000 g, 15 min), and the pellet was resuspended in 1 mL of deuterium-depleted water (DDW). The absorbance spectra of solutions and suspensions were acquired using a TECAN M1000 plate reader. SFB NPs size and zeta potential were quantified via dynamic light scattering (DLS) in the subsequent days following fabrication. Drug loading and encapsulation efficiency of SFB NPs were obtained using HPLC. In brief, acetonitrile precipitation was used for SFB extraction. Separation of SFB was obtained using C18 column of dimensions 150  $\text{mm} \times 2.1$  mm i.d., 3.5  $\mu\text{m}$  (Agilent Technologies USA). This used a mobile phase comprising deionized water and acetonitrile, both containing 0.1% trifluoroacetic acid. The gradient was from 0 to 95% acetonitrile over the course of 17 min and flow rate of 1  $\text{mL min}^{-1}$  and  $\lambda = 280$  nm. Drug loading was calculated by measuring the mass of SFB in NPs compared to the total mass of formed NPs. The used formula is depicted in Equation (1). Encapsulation efficiency was calculated by comparing the mass of SFB in a NP form to the total mass of SFB added, as described by Equation (2).

$$\text{Drug loading (\%)} = 100 \times \left( \frac{\text{mass of SFB in NPs (mg)}}{\text{total mass of NPs (mg)}} \right) \quad (1)$$

$$\text{Encapsulation efficiency (\%)} = 100 \times \left( \frac{\text{mass of SFB in NPs (mg)}}{\text{total mass of SFB added (mg)}} \right) \quad (2)$$

**U87 Cell Cultures:** U87 GBM cells were cultured in full medium, MEM-Eagle supplemented with 10% fetal calf serum (FCS), 2% L-glutamine, and 0.05% gentamycin (Biological Industries, Beit Ha'emek, Israel) at 37 °C in 5%  $\text{CO}_2$  incubator. The culture medium was changed every 2 days.

**U87 Cell Viability:** U87 cells were seeded ( $5 \times 10^3$  cells well<sup>-1</sup>) in a 96-well plate and treated with drug and/or FUS protocol 24 h postplate seeding. The drug treatment consisted of applying multiple concentrations (0.0004, 0.0012, 0.0037, 0.01, 0.03, and 0.1  $\text{mg mL}^{-1}$ ) of SFB NPs or SFB in its free form to triplicate well plates. Following 72 h postdrug incubation, cell viability was assessed using MTT assay. In brief, the assay composed of seeding U87 cells into the 96-well plates. Following incubation for 24 h, the cells were exposed to different SFB NPs concentrations and/or ultrasonic treatment and kept at 37 °C for 72 h. Then, MTT solution in a concentration of 0.5  $\text{mg mL}^{-1}$  was added into each well and incubated with cells for 4 h prior to reading absorbance via a microplate reader (Thermo Multiskan MK3, USA) for cell viability analysis. In the case of free dye, U87 cells were seeded ( $2 \times 10^4$  cells well<sup>-1</sup>) in a 96-well plate and treated with multiple concentrations of free dye for 48 h. Then, cell viability was assessed using the MTS assay. All the experiments were performed in triplicates.

**Tumor Spheroids:** U87 cells were cultured in ultralow attachment flasks, enabling adhesive forces between cells to overcome the interaction between the cells and the flask surface. Plates of 96 wells were used for cell growth 72 h prior to drug and/or FUS treatment (described in U87 Cell Cultures section). The same protocol detailed below for 2D cell cultures was also applied in the case of 3D spheroids. Cell viability was assessed using Cell-titer-Glo (Promega, Wisconsin, USA). To assess the viability of the spheroids, the cells were incubated with a ratio of 1:1 of medium and the reagent for 2 min in an orbital shaker to induce lysis and were then left for 10 min for the luminescent signal to stabilize. Luminescence was recorded using a Synergy H1 (BioTek) plate reader. ImageJ (NIH) was used to quantify the visible spheroid area following treatments.

**In Vitro FUS Setup:** For the in vitro experiments employing a combined treatment of SFB NPs with FUS, a 1 MHz FUS transducer was positioned below each well plate so that the bottom of the cell plate was covered by the acoustic field. Acoustic gel was used as coupling medium between the probe and the plate. The pressure at the bottom of the plate was approximately 0.9 MPa, as measured by an acoustic hydrophone (Onda). The acoustic protocol used in the in vitro experiments included transmitting pressure waves with pulse repetition frequency (PRF) of 1 Hz, pulse length of 50 ms and a total sonication time of 90 s. This protocol was applied sequentially onto each well plate used for assessing the FUS + SFB NPs combination treatment or FUS treatment only.

**SFB NPs Uptake by U87 Cells and Its Pro-Apoptotic Effect:** The uptake of SFB NPs by U87 cells was quantified via flow cytometric analysis of cells emitting the IR783 fluorescence upon SFB NPs treatment at three different concentrations: 0, 2, and 10  $\mu\text{g mL}^{-1}$ . Specifically, on the treatment day, cells were trypsinized and concentrated in aliquots of 140  $\mu\text{L}$  containing  $4.5 \times 10^5$  cells. The aliquots were grouped into the three SFB NPs concentrations, in triplicates, and left in coincubation for approximately 1 h prior to flow preparation. The preparation of cells for flow cytometry composed of centrifuging the cells (4 °C, 350 g and 5 min), and substituting their supernatant with cell staining buffer (CSB). This was repeated 3 times before using fixation buffer to fix the cells. Cells were washed twice after fixation and kept at 4 °C, in the dark, until flow cytometric imaging. This same procedure was adopted when treating cells with FUS sonication and SFB NPs treatment. The relevant aliquots were sonicated for 90 s using the same FUS apparatus used in the in vivo studies, by colocalizing the aliquot content with the acoustic focal zone. In some aliquots, MBs (Sonovue) were added immediately prior to sonication reaching a final concentration of 4.26  $\mu\text{L}/1$  mL ([MBs]/[Total solution volume]). Flow cytometric analysis was used for apoptosis quantification of U87 cells following incubation with either free SFB NPs or SFB (dose matched based on drug loading), and compared to no treatment. In brief, preseeded ( $5 \times 10^5$  cells well<sup>-1</sup> in a 6 well plate) cells were dosed and left for 24 h at 37 °C. Then, cells were washed and stained for Annexin-V-FITC and propidium iodide following a commercial kit protocol (ThermoFisher).



**Animal Studies:** The animal studies were conducted in accordance with a protocol approved by the Animal Care and Use Committee (ACUC) of the Ruth and Bruce Rappaport Faculty of Medicine, Technion Institute of Technology, Haifa, Israel (IL-022-02-2020). The protocol followed the guidelines of the National Institutes of Health (NIH) IC ACUC.

**In Vivo FUS-Mediated BBB Disruption:** The experimental setup for the in vivo ultrasonic studies used a stereotaxic apparatus (Stoelting) platform to accurately position the ultrasonic probe atop the mice's head. The FUS connected to this system was a 1 MHz ultrasound probe (Mettler Electronics), to which a specially designed acoustic lens was attached (focal distance = 4 mm). During procedure, mice were continuously anesthetized using 1–3% Isoflurane, via a facial mask, following positioning in the stereotaxic platform. The mice skulls were first shaved. Then, an ultrasound coupling gel was smeared atop the skull. Subsequently, the stereotaxic arm containing the ultrasonic device was positioned atop the targeted region (coordinates: 1.5 mm to the left and 2.5 mm upward the lambda point, and at a 2.5 mm depth as measured from the cortical bone), so that the acoustic focal spot matched the selected brain target. Each mouse was intravenously administered a solution comprising of 10  $\mu$ L Sonovue (Bracco Imaging) diluted with an additional 140  $\mu$ L of saline, immediately prior to the application of the sonication protocol. The estimated peak negative pressure at the cerebral focal zone was 0.8 MPa, measured using an acoustic hydrophone (Onda) in a water tank and taking into consideration the skull-induced attenuation effect.<sup>[60]</sup> The acoustic pulse length was of 50 ms, with pulse repetition frequency of 1 Hz. FUS-mediated BBB disruption was applied with a duration of 60 s. In some of the animals, a small skin incision was applied atop the skull to accurately identifying the targeted region for the BBB disruption. Following ultrasound treatment, for experiments assessing successful BBB disruption, SFB NPs at a concentration of 20 mg kg<sup>-1</sup> were intravenously administered immediately postsonication. The mice were then euthanized 1 h postinjection for further tissue analysis.

**Stereotaxic Inoculation of U87 Tumors:** The inoculation of the U87 cells was performed using the Stereotaxic equipment (Stoelting). Male SCID mice, 6 weeks old (cat.C.B-17/1crHsd-Prkdc-scid-lyst-bg-j, Envigo, Rehovot, Israel), were first anesthetized using a cocktail of ketamine and xylazine, diluted in saline (ketamine 100 mg kg<sup>-1</sup>; xylazine 5 mg kg<sup>-1</sup>). Following animal positioning into the stereotaxic apparatus, a 1 cm sagittal incision was made over the parieto-occipital bone. The exposed skull surface was then sterilized with iodine solution. Next, U87 cells (3.5–5.0  $\times 10^5$  in 5  $\mu$ L) were injected intracranially, at the coordinates of 1.5 mm left and 2.5 mm upward the lambda zone, and at 2.5 mm depth measured from the cortical bone. Following intracranial surgery, the mice were administered with buprenorphine subcutaneously.

**Bioluminescence and Fluorescence Imaging with Lumina X5 IVIS Imaging:** IVIS imaging was used to assess SFB NPs accumulation in the brain (radiant efficiency) and to assess tumor growth (bioluminescence). To assess tumor growth, luciferin (D-Luciferin potassium salt, 150 mg kg<sup>-1</sup>) was intraperitoneally administered to the animals prior to imaging, and images were acquired every 2 min until the detected signal peaked. The tumor cell line used in this research (U87-Luc) was transfected with a plasmid encoding for the enzyme luciferase, enabling the conversion of the chemical energy into photons with resultant emission of light. Following intraperitoneal administration of luciferin, the mice were anesthetized with isoflurane (1–2%). Measurements were conducted every 2 min for up to 30 min after luciferin injection. Bioluminescence monitoring was conducted up to 3 times a week after cell inoculation into the brain. The parameters used during bioluminescence imaging were: exposure time = 2 s, binning = medium,  $F/F_{stop} = 1$ , field of view = "C."

The fluorescence mode was applied to assess SFB NPs accumulation in the brain and other organs utilizing 0.6 s of exposure time, binning = small and  $F/F_{stop} = 4$ , and excitation and emission wavelengths of 740 and 790 nm, respectively. Regions of interest (ROI) encompassing the intracranial cavity were defined using Living Image software (Perkin Elmer, Waltham, MA), and the efficiency was recorded in (photons/sec/cm<sup>2</sup>/steradian/( $\mu$ W cm<sup>-2</sup>)). The same protocol was applied for the SFB NPs biodistribution analysis, but using photon counts as units.

**Fluorescence Microscopy Imaging:** Fluorescence microscopy was used to visually assess SFB NP extravasation into the brain parenchyma. Following the FUS-mediated BBB disruption protocol described above, brain slides from mice either receiving an intravenous injection of SFB NPs at 30 mg kg<sup>-1</sup> following FUS application or SFB NPs-only injection were acquired (control). The slides were prepared by euthanizing the mice, approximately 1 h posttreatment, and fixating the brains in a 4% formaldehyde solution for 4 days followed by cryoprotection with 25% sucrose. Then, coronal sections (20  $\mu$ m in thickness) were sliced using a Leica CM 3050S-cryostat (Leica Microsystems Nussloch GmbH, Nussloch, Germany) collected and dried on glass slides. Fluorescent images were acquired using the Panoramic 250 Flash III automated digital scanner (3D Histech Ltd., Budapest, Hungary) using a 20X/0.8 Plan Achromat objective for fluorescence with a Cy7 filter (LED 720/30, Excitation 708/75, Emission 809/81) and Cy2 filter (LED 475/28, Excitation 485/26, Emission 521/27) for autofluorescence visualization.

**Statistical Analysis:** GraphPad Prism version 9 for Macintosh (Graph-Pad Software, San Diego, CA) was used for statistical analysis implementing two-tailed unpaired t-test and one- or two-way analysis of variance (ANOVA), as appropriate. The results are expressed as mean  $\pm$  SEM and  $p < 0.05$  was considered statistically significant. Some graphics displayed in this article were generated using Biorender software.

## Supporting Information

Supporting Information is available from the Wiley Online Library or from the author.

## Acknowledgements

The authors would like to acknowledge and thank the help of Mr. Paul from the Technion Animal center with animal handling and Mr. Aharon Alfasi for his technical support during the experiments. Further, the authors appreciate Ms. Maya Holdengreber, Ms. Melia Gurewitz, and Ms. Esther Messer for their support with fluorescence imaging and analysis. The authors would like to thank Professor Khalid Shah for his help with the cell lines used in this article. This work was funded by the Technion Institute of Technology, the MIT-Israel Zuckerman STEM Fund (grant no. 2214110), the Technion Integrated Cancer Center, and the Binational Science Fund—Prof. Rahamimoff Travel grant.

## Conflict of Interest

The authors declare no conflict of interest.

## Data Availability Statement

The data that support the findings of this study are available from the corresponding author upon reasonable request.

## Keywords

blood–brain barrier (BBB), focused ultrasound, glioblastoma, nanoparticles, sorafenib

Received: September 9, 2022

Revised: October 25, 2022

Published online:

- [1] C. Adamson, O. O. Kanu, A. I. Mehta, C. Di, N. Lin, A. K. Mattox, D. D. Bigner, *Expert Opin. Invest. Drugs* **2009**, *18*, 1061.
- [2] Q. T. Ostrom, H. Gittleman, P. Farah, A. Ondracek, Y. Chen, Y. Wolinsky, N. E. Stroup, C. Kruchko, J. S. Barnholtz-Sloan, *Neuro-Oncol.* **2013**, *18*, 1061.
- [3] R. Stupp, W. P. Mason, M. J. Van Den Bent, M. Weller, B. Fisher, M. J. B. Taphoorn, K. Belanger, A. A. Brandes, C. Marosi, U. Bogdahn, J. Curschmann, R. C. Janzer, S. K. Ludwin, T. Gorlia, A. Allgeier, D. Lacombe, J. G. Cairncross, E. Eisenhauer, R. O. Mirimanoff. *N. Engl. J. Med.* **2005**, *352*, 987
- [4] T. H. M. Keegan, L. A. G. Ries, R. D. Barr, A. M. Geiger, D. V. Dahlke, B. H. Pollock, W. A. Bleyer, *Cancer* **2016**, *122*, 1009.
- [5] C. Anderson, H. B. Nichols, *JNCI J. Natl. Cancer Inst.* **2020**, *112*, 994.
- [6] A. C. Tan, D. M. Ashley, G. Y. López, M. Malinzak, H. S. Friedman, M. Khasraw, *CA Cancer J. Clin.* **2020**, *70*, 299.
- [7] C. D. Arvanitis, G. B. Ferraro, R. K. Jain, *Nat. Rev. Cancer* **2020**, *20*, 26.
- [8] D. Furtado, M. Björnholm, S. Ayton, A. I. Bush, K. Kempe, F. Caruso, *Adv. Mater.* **2018**, *30*, 1801362.
- [9] O. Van Tellingen, B. Yetkin-Arik, M. C. De Gooijer, P. Wesseling, T. Wurdinger, H. E. De Vries, *Drug Resist. Updates* **2015**, *19*, 1.
- [10] P. C. De Witt Hamer. *Neuro-Oncology* **2010**, *12*, 304.
- [11] C. Alamón, B. Dávila, M. F. García, C. Sánchez, M. Kovacs, E. Trias, L. Barbeito, M. Gabay, N. Zeineh, M. Gavish, F. Teixidor, C. Viñas, M. Couto, H. Cerecetto, *Cancers* **2020**, *12*, 3423.
- [12] S. M. Wilhelm, L. Adnane, P. Newell, A. Villanueva, J. M. Llovet, M. Lynch, *Mol. Cancer Ther.* **2008**, *7*, 3129
- [13] Y. Shamay, J. Shah, M. A. İşık, A. Mizrahi, J. Leibold, D. F. Tschaharganeh, D. Roxbury, J. Budhathoki-Uprety, K. Nawaly, J. L. Sugarman, E. Baut, M. R. Neiman, M. Dacek, K. S. Ganesh, D. C. Johnson, R. Sridharan, K. L. Chu, V. K. Rajasekhar, S. W. Lowe, J. D. Chodera, D. A. Heller. *Nat. Mater.* **2018**, *17*, 361
- [14] Y. Jo, E. Kim, S. Sai, J. Kim, J.-M. Cho, H. Kim, J.-H. Baek, J.-Y. Kim, S.-G. Hwang, M. Yoon, *Int. J. Mol. Sci.* **2018**, *19*, 3684
- [15] F. Broekman, *World J. Clin. Oncol.* **2011**, *2*, 80.
- [16] A. F. Hottinger, A. B. Aissa, V. Espeli, D. Squiban, N. Dunkel, M. I. Vargas, T. Hundsberger, N. Mach, K. Schaller, D. C. Weber, A. Bodmer, P.-Y. Dietrich, *Br. J. Cancer* **2014**, *110*, 2655.
- [17] M. D. Siegelin, C. M. Raskett, C. A. Gilbert, A. H. Ross, D. C. Altieri, *Neurosci. Lett.* **2010**, *478*, 165.
- [18] J. D. Hainsworth, T. Ervin, E. Friedman, V. Priego, P. B. Murphy, B. L. Clark, R. E. Lamar, *Cancer* **2010**, *116*, 3663.
- [19] E. Q. Lee, J. Kuhn, K. R. Lamborn, L. Abrey, L. M. Deangelis, F. Lieberman, H. I. Robins, S. M. Chang, W. K. A. Yung, J. Drappatz, M. P. Mehta, V. A. Levin, K. Aldape, J. E. Dancey, J. J. Wright, M. D. Prados, T. F. Cloughesy, M. R. Gilbert, P. Y. Wen, *Neuro-Oncol.* **2012**, *14*, 1511.
- [20] E. Galanis, S. K. Anderson, J. M. Lafky, J. H. Uhm, C. Giannini, S. K. Kumar, T. K. Kimlinger, D. W. Northfelt, P. J. Flynn, K. A. Jaeckle, T. J. Kaufmann, J. C. Buckner, *Clin. Cancer Res.* **2013**, *19*, 4816.
- [21] D. M. Peereboom, M. S. Ahluwalia, X. Ye, J. G. Supko, S. L. Hilderbrand, S. Phuphanich, L. B. Nabors, M. R. Rosenfeld, T. Mikkelsen, S. A. Grossman, *Neuro-Oncol.* **2013**, *15*, 490.
- [22] P. L. Nghiemphu, V. A. Ebian, P. Wen, M. Gilbert, L. E. Abrey, F. Lieberman, L. M. Deangelis, H. I. Robins, W. K. A. Yung, S. Chang, J. Drappatz, M. P. Mehta, V. A. Levin, K. Aldape, J. E. Dancey, J. J. Wright, M. Prados, J. Kuhn, T. F. Cloughesy, *J. Neurooncol.* **2018**, *136*, 79.
- [23] C. Jin, K. Wang, A. Oppong-Gyebi, J. Hu, *Int. J. Med. Sci.* **2020**, *17*, 2964.
- [24] C. G. Patil, D. G. Walker, D. M. Miller, P. Butte, B. Morrison, D. S. Kittle, S. J. Hansen, K. L. Nufer, K. A. Byrnes-Blake, M. Yamada, L. L. Lin, K. Pham, J. Perry, J. Parrish-Novak, L. Ishak, T. Prow, K. Black, A. N. Mamelak, *Clin. Neurosurg.* **2019**, *85*, E641.
- [25] S. S. Cho, S. Sheikh, C. W. Teng, J. Georges, A. I. Yang, E. De Ravin, L. Buch, C. Li, Y. Singh, D. Appelt, E. J. Delikatny, E. J. Petersson, A. Tsourkas, J. Dorsey, S. Singhal, J. Y. K. Lee, *Mol. Imaging Biol.* **2020**, *22*, 1266.
- [26] E. H. Kim, J. M. Cho, J. H. Chang, S. H. Kim, K. S. Lee, *Acta Neurochir.* **2011**, *153*, 1487.
- [27] B. Halle, K. Mongelard, F. Poulsen, *Asian J. Neurosurg.* **2019**, *14*, 5.
- [28] J. Zhang, C. Chen, A. Li, W. Jing, P. Sun, X. Huang, Y. Liu, S. Zhang, W. Du, R. Zhang, Y. Liu, A. Gong, J. Wu, X. Jiang, *Nat. Nanotechnol.* **2021**, *16*, 538
- [29] A. Galstyan, J. L. Markman, E. S. Shatalova, A. Chiechi, A. J. Korman, R. Patil, D. Klymyshyn, W. G. Tourtellotte, L. L. Israel, O. Braubach, V. A. Ljubimov, L. A. Mashouf, A. Ramesh, Z. B. Grodzinski, M. L. Penichet, K. L. Black, E. Holler, T. Sun, H. Ding, A. V. Ljubimov, J. Y. Ljubimova, *Nat. Commun.* **2019**, *10*, 3850.
- [30] M. Gabay, A. Weizman, N. Zeineh, M. Kahana, F. Obeid, N. Allon, M. GavishCell. *Mol. Neurobiol.* **2021**, *41*, 1019.
- [31] S. I. Rapoport, *Expert Opin. Investig. Drugs* **2001**, *10*, 1809
- [32] R. A. Kroli, E. A. Neuwelt, E. A. Neuwelt, *Neurosurgery* **1998**, *42*, 1083
- [33] K. Chung, I. Ullah, N. Kim, J. Lim, J. Shin, S. C. Lee, S. Jeon, S. H. Kim, P. Kumar, S.-K. Lee, *J. Drug Targeting* **2020**, *28*, 617
- [34] X. Zhang, G. Chen, L. Wen, F. Yang, A.-L. Shao, X. Li, W. Long, L. Mu, *Eur. J. Pharm. Sci.* **2013**, *48*, 595.
- [35] X. Yi, D. S. Manickam, A. Brynskikh, A. V. Kabanov, *J. Controlled Release* **2014**, *190*, 637.
- [36] V. Askoxylakis, C. D. Arvanitis, C. S. F. Wong, G. B. Ferraro, R. K. Jain, *Adv. Drug Delivery Rev.* **2017**, *119*, 159.
- [37] K.-C. Wei, P.-C. Chu, H.-Y. J. Wang, C.-Y. Huang, P.-Y. Chen, H.-C. Tsai, Y.-J. Lu, P.-Y. Lee, I.-C. Tseng, L.-Y. Feng, P.-W. Hsu, T.-C. Yen, H.-L. Liu, X. He, *PLoS One* **2013**, *8*, e58995.
- [38] A. Idbaih, M. Canney, L. Belin, C. Desseaux, A. Vignot, G. Bouchoux, N. Asquier, B. Law-Ye, D. Leclercq, A. Bissery, Y. De Rycke, C. Trosch, L. Capelle, M. Sanson, K. Hoang-Xuan, C. Dehais, C. Houillier, F. Laigle-Donadey, B. Mathon, A. André, C. Lafon, J.-Y. Chapelon, J.-Y. Delattre, A. Carpentier, *Clin. Cancer Res.* **2019**, *25*, 3793
- [39] C.-Y. Ting, C.-H. Fan, H.-L. Liu, C.-Y. Huang, H.-Y. Hsieh, T.-C. Yen, K.-C. Wei, C.-K. Yeh, *Biomaterials* **2012**, *33*, 704
- [40] K. Hynynen, N. Mcdannold, N. Vykhdotseva, F. A. Jolesz, *Radiology* **2001**, *220*, 640
- [41] A. B. Etame, R. J. Diaz, M. A. O'reilly, C. A. Smith, T. G. Mainprize, K. Hynynen, J. T. Rutka, *Nanomed. Nanotechnol. Biol. Med.* **2012**, *8*, 1133.
- [42] F.-Y. Yang, T.-T. Wong, M.-C. Teng, R.-S. Liu, M. Lu, H.-F. Liang, M.-C. Wei, *J. Controlled Release* **2012**, *160*, 652.
- [43] M. C. Rich, J. Sherwood, A. F. Bartley, Q. A. Whitsitt, M. Lee, W. R. Willoughby, L. E. Dobrunz, Y. Bao, F. D. Lubin, M. Bolding, *J. Controlled Release* **2020**, *324*, 172.
- [44] M. Aryal, N. Vykhdotseva, Y.-Z. Zhang, J. Park, N. Mcdannold, *J. Controlled Release* **2013**, *169*, 103
- [45] T. Kobus, N. Vykhdotseva, M. Pilatou, Y. Zhang, N. Mcdannold, *Ultrasound Med. Biol.* **2016**, *42*, 481
- [46] F. Zustovich, L. Landi, G. Lombardi, L. Galli, C. Porta, D. Amoroso, A. Fontana, M. Andreuccetti, C. Galli, A. Falcone, V. Zagonel, *Anticancer Res.* **2011**, *29*, 2080.
- [47] E. Carra, F. Barbieri, D. Marubbi, A. Pattarozzi, R. E. Favoni, T. Florio, A. Daga, *Cell Cycle* **2013**, *12*, 491.
- [48] J.-Y. Kim, Y. Jo, H.-K. Oh, E. H. Kim, *Am. J. Cancer Res.* **2020**, *10*, ISSN 2156-6976/PMID 33163284.
- [49] Y. Imamura, T. Mukohara, Y. Shimono, Y. Funakoshi, N. Chayahara, M. Toyoda, N. Kiyota, S. Takao, S. Kono, T. Nakatsura, H. Minami, *Oncol. Rep.* **2015**, *33*, 1837.

- [50] C. Berrouet, N. Dorilas, K. A. Rejniak, N. Tuncer, *Bull. Math. Biol.* **2020**, *82*, 079285.
- [51] M. J. Mitchell, M. M. Billingsley, R. M. Haley, M. E. Wechsler, N. A. Peppas, R. Langer, *Nat. Rev. Drug Discovery* **2021**, *20*, 101.
- [52] Y.-Z. Zhao, Y.-K. Luo, C.-T. Lu, J.-F. Xu, J. Tang, M. Zhang, Y. Zhang, H.-D. Liang, *J. Drug Targeting* **2008**, *16*, 18.
- [53] P. Qin, T. Han, A. C. H. Yu, L. Xu, *J. Controlled Release* **2018**, *272*, 169.
- [54] T. Ilovitsh, Y. Feng, J. Foiret, A. Kheirloomoom, H. Zhang, E. S. Ingham, A. Ilovitsh, S. K. Tumbale, B. Z. Fite, B. Wu, M. N. Raie, N. Zhang, A. J. Kare, M. Chavez, L. S. Qi, G. Pelled, D. Gazit, O. Vermesh, I. Steinberg, S. S. Gambhir, K. W. Ferrara, *Proc. Natl. Acad. Sci. U.S.A.* **2020**, *117*, 12674.
- [55] H. Maeda, J. Wu, T. Sawa, Y. Matsumura, K. Hori, *J. Controlled Release* **2000**, *65*, 271.
- [56] J. S. Suk, Q. Xu, N. Kim, J. Hanes, L. M. Ensign, *Adv. Drug Delivery Rev.* **2016**, *99*, 28.
- [57] L. Marrero, D. Wyczechowska, A. E. Musto, A. Wilk, H. Vashistha, A. Zapata, C. Walker, C. Velasco-Gonzalez, C. Parsons, S. Wieland, D. Leviitt, K. Reiss, O. Prakash, *Neoplasia* **2014**, *16*, 874.
- [58] M. Candolfi, J. F. Curtin, W. Stephen Nichols, A. K. M. G. Muhammad, G. D. King, G. Elizabeth Pluhar, E. A. McNiel, J. R. Ohlfest, A. B. Freese, P. F. Moore, J. Lerner, P. R. Lowenstein, M. G. Castro, *Bone* **2008**, *23*, 1.
- [59] a) M. Gabay, A. Weizman, N. Zeineh, M. Kahana, F. Obeid, N. Allon, M. Gavish, *Cell. Mol. Neurobiol.* **2021**, *41*, 1019; b) M. Gabay, A. Weizman, N. Zeineh, M. Kahana, F. Obeid, N. Allon, M. Gavish, *Cell. Mol. Neurobiol.* **2022**, *42*, 1265.
- [60] J. J. Choi, M. Pernot, S. A. Small, E. E. Konofagou, *Ultrasound Med. Biol.* **2007**, *33*, 95.